Brief Articles

NMR Structure of a Potent Small Molecule Inhibitor Bound to Human Keratinocyte Fatty Acid-Binding Protein†

Patricia A. McDonnell,* Keith L. Constantine, Valentina Goldfarb, Stephen R. Johnson, Richard Sulsky, David R. Magnin, Jeffrey A. Robl, Thomas J. Caulfield, Rex A. Parker, David S. Taylor, Leonard P. Adam, William J. Metzler, Luciano Mueller, and Bennett T. Farmer, II‡

Bristol-Myers Squibb Pharmaceutical Research Institute, P.O. Box 4000, Princeton, New Jersey 08543

Received March 28, 2006

The NMR structure is presented for compound **1** (BMS-480404) (K_i = 33 (±2) nM) bound to keratinocyte fatty acid-binding protein. This article describes interactions between a high affinity drug-like compound and a member of the fatty acid-binding protein family. A benzyl group ortho to the mandelic acid in **1** occupies an area of the protein that fatty acids do not normally contact. Similar to that in the kFABP−palmitic acid structure, the acid moiety in **1** is proximal to R129 and Y131. Computational modeling indicates that the acid moiety in **1** interacts indirectly via a modeled water molecule to R109.

Introduction

Lipid-binding proteins are a family of small, cytosolic proteins that modulate fatty acid storage, trafficking, and solubilization. Members of this family share a conserved structural topology, with sequence identities ranging from 20 to 70%. Family members are grouped according to their sequence homology and ligand binding characteristics. Common ligands include long-chain fatty acids, bile acids, retinoids, and eicosanoids. Lipid-binding proteins have a highly conserved folding motif despite exhibiting various affinities for amphiphilic ligands. The common tertiary structure consists of a ten-stranded β-barrel with a large central cavity capped by a helix-turn-helix motif partially covering the internal water-filled cavity.[1] Most NMR and X-ray crystal structures of proteins in this class are of the apo protein or of a protein/fatty acid complex.[2−4] The lipid-binding cavity contains both polar and nonpolar residues, and in some lipid-binding proteins, highly conserved tyrosine and arginine residues form hydrogen bonds with the carboxylate end of a fatty acid.[4−7] The cooperative binding of weak ligands in human ileal bile acid-binding protein[8] lends support to the idea that tight inhibitors can be designed against fatty acid-binding proteins. Recently, a crystal structure of human adipocyte lipid-binding protein (aP2, ALBP, FABP4[a]) in complex with a lead-like small molecule (EC_{50} ~10μM) was reported.[9] A combination of NMR screening, computational methods and X-ray crystallography identified a submicromolar lead compound for aP2.[10] This article reports the structure of a potent (K_i = 33 (±2) nM) small molecule inhibitor bound to a member of the lipid-binding protein family.

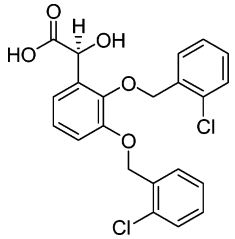

Figure 1. Structure of **1**, which has a K_i of 33 (±2) nM for kFABP as determined by the displacement of bound 1-anilinonaphthalene-8-sulfonic acid (1,8-ANS).[19]

Adipocytes express two lipid-binding proteins, aP2 (the major protein) and keratinocyte fatty acid-binding protein (kFABP, mal-1, FABP5), the minor protein. aP2 is exclusively found in adipocytes, whereas kFABP is found in numerous tissues, including the lens, retina, tongue, lung, brain, skin, and some epithelial and endothelial cells.[11−15] Recent studies suggest that a positive relationship exists between lipolysis and the total lipid-binding protein abundance in adipocytes and that a degree of functional degeneracy exists between kFABP and aP2.[16,17] A compound that potently inhibits aP2 and/or kFABP may provide a therapeutic mechanism for uncoupling insulin resistance and diabetes from obesity.[18]

To assist in the design of potent dual inhibitors of aP2 and kFABP, we determined the structure of **1** (BMS-480404)[18] (Figure 1) in complex with kFABP. Compound **1** is a member of a series of aromatic compounds that act as aP2 inhibitors or dual aP2/kFABP inhibitors and is a potential therapeutic agent for the treatment of metabolic disorders.[18] Because we were unable to obtain diffraction quality crystals of **1** and kFABP, we determined the NMR structure of the complex. This article describes the NMR-derived structure of **1** bound to kFABP and the key interactions the ligand makes in the binding pocket. The NMR structure is used to interpret the observed activity of the analogues of **1**.

Results and Discussion

The NMR structure of kFABP−**1** was determined using a suite of 2D, 3D, and 4D NMR experiments. Under our

† The resonance assignments for kFABP−**1** have been deposited in the BMRB databank, access code 7107.

* To whom correspondence should be addressed. Phone: 609-252-4286. Fax: 609-252-6012. E-mail: patricia.mcdonnell@bms.com.

‡ Present address: Boehringer Ingelheim Pharmaceuticals, Inc., 900 Ridgebury Road, P.O. Box 368, Ridgefield, CT 06877.

[a] Abbreviations: kFABP, mal-1, FABP5, keratinocyte fatty acid-binding protein; aP2, ALBP, FABP4, adipocyte lipid-binding protein; 1,8-ANS, 1-anilinonaphthalene-8-sulfonic acid; HSQC−NOESY, heteronuclear single quantum correlation−nuclear Overhauser spectroscopy; RMSD, root mean-square deviation.

10.1021/jm060360i CCC: $33.50
Published on Web 07/11/2006

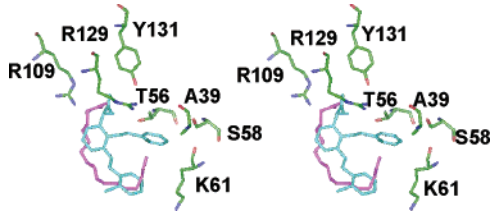

Figure 2. Representative structure of **1** from NMR ensemble data (cyan) superimposed on palmitic acid from X-ray data (magenta). Residues R109, R129, and Y131 typically interact with the acid moiety of the ligand in this family of proteins. A cluster of residues (A39, T56, S58, and K61) have NOEs to the benzyl ring ortho to the mandelic acid.

experimental conditions, the following residues were doubled, indicating a minor conformational state of the protein: D15, S16, L26, G27, G29, R33, D42, F65, F73, D79, G80, R81, T83, V86, and E132. This is similar to what was previously reported.[6] Some of these residues are localized near the binding site; others are distributed throughout the protein structure. The binding of **1** did not affect the relative populations of the major and minor forms of kFABP. Amide resonances were missing for the following residues, which are all surface exposed: T3, G18, K40, T59, T76, D91, D113, and N124. These same observations of doubled and missing resonances were seen in NMR studies of muscle fatty acid-binding protein.[3] The 3D ^{13}C-edited, ^{13}C/^{15}N-filtered HSQC−NOESY, and 2D F_1,F_2-^{13}C/^{15}N-filtered NOE experiments[20] were recorded to obtain intermolecular NOEs between kFABP and **1** and intramolecular NOEs within **1**, respectively. The X-ray crystal structure of kFABP−palmitic acid[21] (pdb entry 1B56) provided a starting conformation for the NMR-restrained annealing calculations[22] of the kFABP−**1** complex. Amide chemical shift perturbation studies indicated that no large conformational change in the protein occurred upon the binding of **1** since shift changes were restricted to mainly the resonances of residues in the active site. Fifty-eight unambiguous and 1 ambiguous intermolecular NOEs and 7 unambiguous ligand intramolecular NOEs were used as restraints during structure calculations. During the initial stages of the structure calculations, all residues were fixed except residues that exhibited NOEs to **1**. In the final minimization, all residues were relaxed. To account for an observed slow exchange behavior of the tyrosine 131 phenolic proton, subsequent rounds of refinement used an ambiguous hydrogen bond restraint between Y131 and the following three ligand oxygens: the two oxygens in the acid moiety and the oxygen from the remaining hydroxyl group. A total of 75 structures were calculated using X-PLOR,[23] from which the 23 lowest energy structures were selected to create an ensemble of structures that satisfied all of the NOE restraints to within 0.15 Å. The ligand heavy atoms had an average root-mean-square deviation (RMSD) of 0.51 Å for these low energy structures in the reference frame of the protein, that is, after superposing the protein backbone atoms.

Figure 2 shows a view of the active site of a selected representative NMR-derived structure of the complex of kFABP−**1** and the previously published X-ray structure of kFABP−palmitic acid. The RMSD in the Cα positions of kFABP−**1** complex is 0.46 Å from the kFABP−palmitic acid complex.[21] The binding cavity of **1** is nearly identical to the cavity observed in the X-ray structure of kFABP−palmitic acid complex. The unbranched portion of **1** matches remarkably well with the hydrocarbon chain of palmitic acid; however, the benzyl group ortho to the mandelic acid in **1** occupies an area that the palmitic acid does not occupy. This portion of **1** is proximal to the side chains of A39, T56, S58, and K61. NOEs are observed between this benzyl group and the following: the methyl of A39, the beta methylene and methyl of T56, the beta methylene of S58, and the beta, delta, and gamma methylenes of K61 (Supporting Information). These contacts indicate that the interaction of the benzyl group ortho to the mandelic acid with kFABP is predominantly hydrophobic as opposed to $\pi-\pi$ stacking. The large difference in the binding affinities between palmitic acid (K_d = 802nM) and **1** (K_i = 33 (±2) nM) may be attributed, in part, to these additional interactions that **1** makes in the kFABP binding pocket. The NMR-derived structure of kFABP−**1** suggests that this cavity can accommodate small substitutions on this aromatic ring such as other halogens or methyl groups in all positions. The synthesis of analogues around the aromatic ring of a closely related compound, although tolerated, display no change in potency (data not shown).

In agreement with structures of fatty acid/protein complexes,[2−4] the NMR-derived structure of kFABP−**1** demonstrates the importance of the acid group in forming key interactions between the compound and the protein. In the literature structure of kFABP−palmitic acid, the carboxylic headgroup forms salt bridges with R109 and R129 and a hydrogen bond interaction with Y131 phenolic OH. The interactions between the acid moiety of **1** with R109 and R129 were not directly observed in our NMR experimental data; however, we observed the slow exchange behavior of the Y131 phenolic OH. On the basis of the structure of kFABP−palmitic acid and the initial structures of our complex, we interpreted this as an interaction between the carboxylate moiety or the hydroxy moiety in **1** and the Y131 phenolic OH group; we included an ambiguous hydrogen bond restraint during the later rounds of refinement. Similar orientations of the acid group of **1** and R109/R128/Y131 were observed when the NMR structure calculations were repeated using an explicit hydrogen bond restraint from the Y131 phenolic OH and the three oxygens of **1**. Table 1 presents the distances observed in the 23 low energy NMR structures of the oxygens of the carboxylate and hydroxyl moieties in **1** and hydrogens of R109, R129, and Y131. In addition, the distances from energy minimization calculations using the OPLS2005 force field on the NMR-derived structure of the kFABP−**1** complex are also presented. In these modeling calculations, a water molecule (HOH 214: pdb entry 1B56) near R109, observed in the X-ray structure of kFABP−palmitic acid, was included. Considering that the NMR-derived structures and the modeled structure of kFABP−**1** used two different force fields, the measured distances between the mandelic acid group in **1** and kFABP residues R109, R129, and Y131 are comparable. Two hydrogens in the guanidinium group of R129 and the Y131 phenolic OH group are proximal to the carboxylate oxygens in **1**. The NH_2 distance of R129 to the carboxylate oxygen (Table 1, distance A) in **1** varies from 1.7 to 2.3 Å and has an average distance of 2.0 Å for the 23 NMR structures. The NHε from the guanidinium group of R129 (Table 1, distance B) is 2.0−2.8 Å with an average distance of 2.2 Å from the second carboxylate oxygen in **1** in the NMR-derived structures. The distances in the OPLS2005-minimized model of kFABP−**1** for these protons are 1.5 and 1.6 Å, respectively. The differences in the exact distances may be a reflection of the different force fields used in the calculations and/or may be due to the fact that the NMR-derived structures are not a static representation of the protein−ligand complexes. Besides being proximal to the side chain of R129, the acid group of **1** is near the Y131 phenolic OH. The distance between the carboxylate oxygen of **1** and the hydrogen of the Y131 phenolic OH (Table 1, distance C) range from 1.9 to 2.8 Å in the NMR-derived structures and is 1.6 Å in the

Table 1. Distances between Mandelic Acid Group in **1** and kFABP Residues R109, R129, and Y131 Measured in NMR-Calculated Structures of kFABP−**1** and in OPLS2005-Minimized kFABP−**1**, Including HOH 214 from PDB Entry 1B56

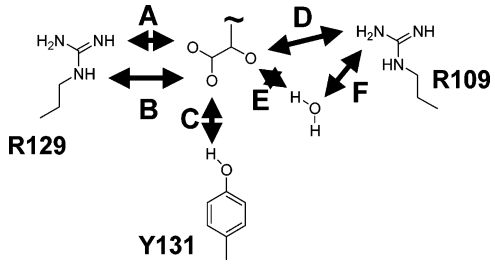

distance[a]	description	range of NMR distances (Å)	modeling distance (Å)
A	R129 NH_2 to **1** oxygen (acid)	1.7−2.3	1.5
B	R129 NHϵ to **1** oxygen (acid)	2.0−2.8	1.6
C	Y131 OH to **1** oxygen (acid)	1.9−2.8	1.6
D	R109 NH_2 to **1** oxygen (hydroxy)	3.0−4.6	3.6
E	**1** oxygen (hydroxy) to water molecule	N.D.[b]	1.7
F	R109 NH_2 to water molecule	N.D.[b]	1.8

[a] Distances reported for 23 lowest energy NMR structures. [b] Not determined because the water molecule was not present during NMR structure calculations.

OPLS2005-minimized structure as shown in Table 1. The data presented in Table 1 demonstrate that the mandelic acid of **1** is proximal to R129 and Y131, in agreement with the kFABP−palmitic acid structure.

The interaction of R109 with the hydroxyl moiety in **1** requires more analysis than simply measuring distances between two atoms. On the basis of the NMR-derived structures of kFABP−**1**, one could conclude that R109 does not interact directly with the hydroxyl moiety of the mandelic acid because the distances observed range from 3.0 to 4.6 Å (Table 1, distance D). One would deduce a similar conclusion on the basis of a direct distance of 3.6 Å between these two atoms in the OPLS2005-minimized kFABP−**1** structure. However, the modeling is consistent with a water-mediated hydrogen bond (HOH 214: pdb entry 1B56) as shown in the kFABP−palmitic acid X-ray structure.[21] A distance of 1.7 Å is observed between the hydroxyl moiety in **1** and the water, and a distance of 1.8 Å is observed between the water and the guanidinium group of R109 as presented in Table 1, distances E and F. In agreement with the kFABP−palmitic acid structure, the data presented in Table 1 indicates that the acid moiety in **1** is proximal to R129 and Y131 and interacts indirectly via a modeled water molecule to R109.

One can use the NMR structure and modeling to interpret the observed activity of the analogues in Table 2. The compounds in Table 2 were selected because they retain the same chain length in the R group with respect to **1**. The compounds were overlaid manually on to the NMR-determined structure of **1**. A crystallographic water (HOH 214: pdb entry 1B56) from the kFABP−palmitic acid X-ray structure was inserted into the NMR structure prior to energy minimization using the OPLS2005 force field (see Experimental Section for details). The replacement of the acid group **1** with a hydroxymethyl group **2** abolishes activity. This data demonstrates that

Table 2. K_i (nM) Binding Constants of **1** Analogues with Substitutions of the Mandelic Acid Moiety

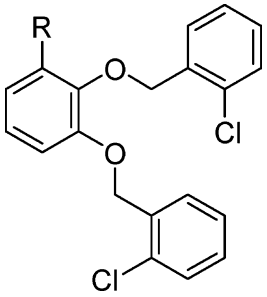

compd	R	kFABP K_i (nM)	aP2 K_i (nM)
1	CH(OH)COOH	33 (±2)	2.5 (±0.1)
2	$CH(OH)CH_2OH$	>2000	>2000
3	$CH(OCH_3)COOH$	9 (±1)	50 (±2)
4	CH_2COOH	3 (±1)	16 (±2)
5	COCOOH	<2[a]	<2[a]

[a] The resolution of the assay does not allow for K_i quantification below 2 nM.

the carboxylate is critical for activity. The replacement of the hydroxyl with a methoxy **3** from **1** results in a gain in activity. Modeling shows that **3** retains the hydrogen bond network to R129, and Y131 and makes the water-mediated hydrogen bond to R109, although the methoxy oxygen is a much poorer acceptor than the hydroxyl. The methoxy group positions itself to make a hydrophobic contact with the methyl of Thr56 while simultaneously relieving the conformational strain on the carboxylate brought about by the internal H bond formed with the hydroxyl of **1**. Combined, these interactions could account for the slight increase in potency relative to that of **1**. The elimination of the hydroxyl group **4** is beneficial for activity. The hydrogen bond network for **4** between R129 and Y131 is retained, but the removal of the hydroxyl group eliminates the indirect hydrogen bond between the inhibitor and the guanidine group of R109. One possible rationalization is that although the hydroxyl is tolerated when it forms a hydrogen bond indirectly via the water molecule to R109, modeling suggests that the hydroxyl of **1** is closer to the methyl of Thr56 creating a hydrophilic/hydrophobic contact. The loss of the indirect hydrogen bond caused by the removal of the hydroxyl is compensated by the release of the intervening water molecule (HOH 214: pdb entry 1B56). Thr56 aligns to a serine in the sequence of aP2; this could account for the higher affinity for **1** verses that for **4** in the case of aP2 (Table 2). The hydroxyl also increases the conformational strain on the carboxylate. The removal of the hydroxyl eliminates both the strain and the disconnect between a hydrophobic and hydrophilic group resulting in the increased potency of **4**. When the hydroxyl group **1** is replaced with a carbonyl **5**, a better hydrogen bond acceptor, binding also increases. The carbonyl now forms both a direct hydrogen bond and a water-mediated hydrogen bond to R109. The hydrogen bond network is retained between R129 and Y131.

Conclusions

The NMR structure of kFABP−**1** (K_i = 33nM) provides a detailed view of a high-affinity, lead-like small molecule bound to a member of the lipid-binding protein family. The 3D structures of this class of proteins typically consist of the apo protein or a protein−fatty acid complex. We performed these NMR studies to assist in the development of potent inhibitors

because we were unable to obtain diffraction quality crystals of compounds in this series and kFABP. The failure to obtain diffraction quality crystals could be a result of the minor heterogeneity that was observed in the NMR spectra.

The NMR structure of kFABP−**1** is similar yet distinct from the X-ray structure of kFABP−palmitic acid. The unbranched portion of **1** matches remarkably well with the hydrocarbon chain of palmitic acid, but a benzyl group ortho to the mandelic acid in **1** occupies an area of the active site that fatty acids do not normally contact. Hydrogen bond interactions involving a carboxylate moiety in a ligand and R109, R129, and Y131 are important as demonstrated in both the X-ray structure of kFABP−palmitic acid and the NMR structure of kFABP−**1**. An interaction between the Y131 phenolic OH and the carboxylate moiety or the hydroxyl moiety is observed directly in the NMR data. The modeling of **1** in the NMR-derived structures including the water molecule near R109 indicate that the hydroxyl moiety of **1** interacts with the NH_2 group of R109 through this crystal water molecule. Combining the NMR-derived structures with the OPLS2005-minimized structure of kFABP−**1**, one concludes that the mandelic acid group in **1** is proximal to R109, R129, and Y131.

The NMR-derived structure of kFABP−**1** can be used to explain the activity of the analogues of **1** and assist in the design of more potent inhibitors. The extreme loss of activity upon the replacement of the acid group with a hydroxymethyl group **2** emphasizes the importance of the carboxylate moiety for activity. When the hydroxyl moiety in the mandelic group in **1** is replaced with an improved hydrogen bond acceptor **5**, the potency increases. The modeling combined with the activity information presented in Table 2 stresses the importance of retaining and forming interactions with R109, R129, and Y131.

A common strategy for obtaining potent inhibitors is to design the inhibitors so that they occupy the same location and satisfy similar interactions as those observed for the native ligand and then selectively build into the surrounding space to pick up additional interactions. This article illustrates the strategy for kFABP. As highlighted by the structure of the kFABP−**1** complex above, our current series of inhibitors fills a similar volume and makes the same pair-wise interactions (with R109, R129, and Y131) as palmitic acid. Large gains in affinity are achieved with the addition of a benzyl moiety ortho to the mandelic acid. The benzyl moiety fills a new region of the protein that is unoccupied by the native ligand. In doing so, the benzyl moiety displaces a water molecule that partially occupies this region (HOH 236: pdb entry 1B56). Water molecules typically occupy extra volume in the binding cavity of fatty acid-binding proteins; for kFABP, a total of eight water molecules reside in the binding cavity (pdb entry 1B56). One can postulate that the judicious removal of other water molecules will result in additional interactions with the protein and lead to a further increase in potency.

Experimental Section

Expression and Purification of kFABP. The human kFABP protein was subcloned into plasmid pET11a (Novagen, Madison, WI) and transformed into *E. coli* BL21 (DE3) (Novagen, Madison, WI). Recombinant *E. coli* were grown on minimal media supplemented with ^{13}C glucose and ^{15}N ammonium sulfate and induced at OD_{600} 1.0 with 0.5 mM isopropyl-β-D-thiogalactopyranoside (MBI Frementas, St. Leon-Rot, Germany) for 2 h at 37 °C. The harvested cells were lysed using sonication in 100 mL of 50 mM Tris-HCl at pH 8.0 and 50mM NaCl supplemented with protease inhibitor cocktail tablets (Roche Diagnostics). The supernatant was applied to a 50 mL Q-Sepharose resin equilibrated with the disruption buffer without the protease inhibitors. The flow-through fraction was chilled and made 40% ammonium sulfate. The solution was spun, and the supernatant was applied to 30 mL of phenyl Sepharose equilibrated 50 mM Tris-HCl at pH 8.0, 50 mM NaCl, and 40% ammonium sulfate. The column was washed with equilibration buffer, and the protein was eluted in 10 mL fractions with a phosphate-buffered saline (PBS) buffer. Fractions containing the protein were concentrated to 30 mL and applied to a Superdex 75 26/60 column equilibrated with PBS, 1 mM EDTA, and 2 mM DTT. Protein-containing fractions were pooled and concentrated. The endogenous lipids were removed from the protein by incubation with prewarmed (50 °C) Lipidex-VI (hydroxyalkoxypropyl dextran-type VI, 10 mL column dimensions). The protein was then exchanged into the NMR buffer of 50 mM Na_2PO_4 at pH 7.5, 50 mM NaCl, 0.1 mM EDTA (d_{12}), 5 mM DTT (d_{10}), 7% D_2O. The typical yield from 1 L of the culture is approximately 40 mg.

NMR Experiments and Sample Preparation. NMR spectra were recorded using a 1:1 complex of 1.4 mM $^{13}C/^{15}N$-labeled kFABP−**1** in the NMR buffer. The samples were approximately 370 μL in a 5 mm micro Shigemi tube. All NMR experiments were carried out at 20 °C on a Varian Inova NMR spectrometer (operating at a 597.76 MHz ^1H frequency) equipped with a Varian 5 mM $^1H/^{13}C/^{15}N$ triple resonance, triple-axis PFG probe.

Resonance assignments were obtained by a combination of computer-assisted (AUTOASSIGN[24]) analyses and semiautomated analyses of the following data sets: 3D HNCO, HNCA, HNCAHA, HNCB, HNHB, HBHACONH, CBCACONH, and HCCH-TOCSY. The modifications to some of the standard pulse sequences has been described previously.[25] The 4D (CN) NOE and (CC) NOE experiments (mix times = 80 and 120 ms, respectively) were recorded to assist with stereoassignments. A gradient enhanced constant-time CH−HSQC experiment was used to measure methyl-CO and methyl-N couplings for the stereospecific assignments of valine, isoleucine, and threonine methyl groups.[26] A gradient enhanced 2D [J_{cc}] double filtered $^1H/^{13}C$ constant time HSQC experiment yielded glycine CA and methionine methyl correlations. The 3D ^{13}C-edited, $^{13}C/^{15}N$-filtered HSQC−NOESY and 2D F_1,F_2-$^{13}C/^{15}N$ -filtered NOE experiments[27] (mix times = 60 and 120 ms) were recorded to obtain interresidue NOEs and intraresidue NOEs. A 2D $^{13}C/^{15}N$ double-reverse-filtered TOCSY experiment (mix time = 27 ms) was used to assist in ligand resonance assignments.

All spectra were processed using a modified version[28] of the FELIX program (Hare Research, Inc.; M. S. Friedrichs, unpublished program), and the residual ^1H_2O signal was removed from all spectra by an application of low-frequency deconvolution[29] in the ^1H acquisition dimension. All ^1H dimensions were referenced relative to the water peak at 4.78 ppm, and ^{13}C and ^{15}N dimensions were referenced indirectly to DSS.[30]

Structure Calculations. The X-ray crystal structure of kFABP−palmitic acid (pdb entry 1B56) provided a starting structure for the NMR-restrained annealing calculations. Specifically, the palmitic acid and crystallographic waters were removed from the pdb file. Initial coordinates from residues 4−134 were used in the NMR structure calculations because resonance assignments were obtained for these residues. Fifty-eight unambiguous and one ambiguous intermolecular NOEs, seven ligand unambiguous intramolecular NOEs, and one ambiguous hydrogen bond were used as restraints during the structure calculations. Stereospecific assignments were made only for some valine, isoleucine, and threonine methyl groups. The dihedral restraints of the chiral center in **1** were used to maintain the ligand in the S configuration. The ligand was randomly translated and rotated prior to the simulated annealing protocol. The protein was fixed except for residues that exhibited NOEs to the ligand during the initial stages of minimization, high-temperature dynamics, and cooling. The entire protein was allowed to relax during the final minimization steps. A total of 75 structures were calculated using X-PLOR from which the 23 lowest energy structures were selected to create an ensemble of structures that satisfied all of the NOE restraints to within 0.15 Å.

The ^{13}C chemical shifts of the C_β residues of all six cysteine residues are consistent with the reduced state,[31] thus we did not include a disulfide bond between C120 and C127 as was observed

in the published crystal structure of kFABP. The differences may reflect the different isolation protocols used by the two groups. Because disulfide bridges are not normally present in intracellular proteins, we added a reducing agent to increase the stability and storage of the protein.

OPLS2005 Minimization Calculations. The compounds in Table 2 were overlayed manually on to the NMR-determined pose of **1**. The crystallographic water (HOH 214: pdb 1B56) from the kFABP−palmitic acid X-ray structure was inserted into the NMR structure. Each compound was energy minimized using the molecular mechanics routine BatchMin, a part of MacroModel,[32] with the OPLS2005 force field and the Generalized-Born/Surface-Area (GB/SA) model.[33] Residues within 7 Å of the ligand were allowed to relax during minimization. All other residues were constrained.

Acknowledgment. We acknowledge Ping Chen for the critical reading of this manuscript.

Supporting Information Available: Structural and Ramachandran plot statistics on the ensemble of the NMR structures of kFABP−**1** and NOE restraints. This material is available free of charge via the Internet at http://pubs.acs.org.

References

(1) Banaszak, L.; Winter, N.; Xu, Z.; Bernlohr, D. A.; Cowan, S.; Jones, T. A. Lipid-Binding Proteins: A Family of Fatty Acid and Retinoid Transport Proteins. *Adv. Protein Chem.* **1994**, *45*, 89−151.

(2) Hodson, M. E.; Ponder, J. W.; Cistola, D. P. The NMR Solution Structure of Intestinal Fally Acid-Binding Protein Complexed with Palmitate: Application of a Novel Distance Geometry Algorithm. *J. Mol. Biol.* **1996**, *264*, 585−602.

(3) Constantine, K. L.; Friedrichs, M. S.; Wittekind, M.; Jamil, H.; Chu, C.; Parker, R. A.; Goldfarb, V.; Mueller, L.; Farmer, B. T. Backbone and Side Chain Dynamics of Uncomplexed Human Adipocyte and Muscle Fatty Acid-Binding Proteins. *Biochemistry* **1998**, *37*, 7965−7980.

(4) Reese-Wagoner, A.; Thompson, J.; Banaszak, L. Structural Properties of the Adipocyte Lipid Binding Protein. *Biochim. Biophys. Acta* **1999**, *1441*, 106−116.

(5) Kane, D. D.; Coe, N. R.; Vanlandingham, B.; Krieg, P.; Bernlohr, D. A. Expression, Purification, and Lignad-Binding Analysis of Recombinant Keratinocyte Lipid-Binding Protein (MAL-1), an Intracellular Lipid-Binding Protein Found Overexpressed in Neoplastic Skin Cells. *Biochemistry* **1996**, *35*, 2894−2900.

(6) Gutierrez-Gonzalez, L. H.; Ludwig, C.; Hohoff, C.; Rademacher, M.; Hanhoff, T.; Ruterjans, H.; Spener, F.; Lucke, C. Solution Structure and Backbone Dynamics of Human Epidermal-Type Fatty Acid-Binding Protein (E-FABP). *Biochem. J.* **2002**, *364*, 725−737.

(7) Zanotti, G. Muscle Fatty Acid-Binding Protein. *Biochimica Biophysica Acta*. **1999**, *1441*, 94−105.

(8) Tochtrop, G. P.; Richter, K.; Tang, C.; Toner, J. J.; Covey, D. F.; Cistola, D. P. Energetics by NMR: Site-Specific Binding in a Positively Cooperative System. *Proc. Natl. Acad. Sci. U.S.A.* **2002**, *99*, 1847−1852.

(9) van Dongen, M. J. P.; Uppenberg, J.; Svensson, S.; Lundback, T.; Akerud, T.; Wikstrom, M.; Schultz, J. Structure-Based Screening as Applied to Human FABP4: A Highly Efficient Alternative to HTS for Hit Generation. *J. Am. Chem. Soc.* **2002**, *124*, 11874−11880.

(10) Moore, J.; Abdul-Manan, N.; Fejzo, J.; Jacobs, M.; Lepre, C.; Peng, J.; Xie, X. Leveraging Structural Approaches: Applications of NMR-Based Screening and X-ray Crystallography for Inhibitor Design. *J. Synchrotron Radiat.* **2004**, *11*, 97−100.

(11) Krieg, P.; Feil, S.; Furstenberger, G.; Bowden, G. T. Tumor-Specific Overexpression of a Novel Keratinocyte Lipid-Binding Protein. Identification and Characterization of a Cloned Sequence Activated During Multistage Carcinogenesis in Mouse Skin. *J. Biol. Chem.* **1993**, *268*, 17362−17369.

(12) Owada, Y.; Yoshimoto, T.; Kondo, H. Increased Expression of the mRNA for Brain- and Skin-Type but Not Heart-type Fatty Acid Binding Proteins Following Kainic Acid Systemic Administration in the Hippocampal Glia of Adult Rats. *Brain Res. Mol. Brain Res.* **1996**, *42*, 156−160.

(13) Jaworski, C.; Wistow, G. LP2, A Differentiation-Associated Lipid-Binding Protein Expressed in Bovine Lens. *Biochem. J.* **1996**, *320*, 49−54.

(14) De Leon, M.; Welcher, A. A.; Nahin, R. H.; Liu, Y.; Ruda, M. A.; Shotter, E. M.; Molina, C. A. Fatty Acid Binding Protein is Induced in Neurons of the Dorsal Root Ganglia after Peripheral Nerve Injury. *J. Neurosci. Res.* **1996**, *44*, 283−292.

(15) Hertzel, A. V.; Bernlohr, D. A. The Mammalian Fatty Acid-Binding Protein Multigene Family: Molecular and Genetic Insights into Function. *Trends Endocrinol. Metab.* **2000**, *11*, 175−180.

(16) Hertzel, A. V.; Bennaars-Eiden, A.; Bernlohr, D. A. Increased Lipolysis in Transgenic Animals Overexpressing the Epithelial Fatty Acid Binding Protein in Adipose Cells. *J. Lipid Res.* **2002**, *43*, 2105−2111.

(17) Coe, N. R.; Simpson, M. A.; Bernlohr, D. A. Targeted Disruption of the Adipocyte Lipid-Binding Protein (aP2 Protein) Gene Impairs Fat Cell Lipolysis and Increases Cellular Fatty Acid Levels. *J. Lipid Res.* **1999**, *40*, 967−972.

(18) Magnin, D. R.; Sulsky, R. B.; Robl, J. A.; Caulfield, T. J.; Parker, R. A. Dual Inhibitors of Adipocyte Fatty Acid Binding Protein and Keratinocyte Fatty Acid Binding Protein. W.O. Patent 03,043,624, 2003.

(19) Kurian, E.; Kirk, W. R.; Prendergast, F. B. Affinity of Fatty Acid for Rat Intestinal Fatty Acid Binding Protein: Further Examination. *Biochemistry* **1996**, *35*, 3865−3874.

(20) Petros, A. M.; Kawai, M.; Luly, J. R.; Fesik, S. W. Conformation of T2o Non-Immunosuppressive FK506 Analogs When Bound to FKBP by Isotope-Filtered NMR. *FEBS Lett.* **1992**, *308*, 309−314.

(21) Hohoff, C.; Borchers, T.; Rustow, B.; Spener, F.; van Tilbeurgh, H. Expression, Purification, and Crystal Structure Determination of Recombinant Human Epidermal-Type Fatty Acid Binding Protein. *Biochemistry* **1999**, *38*, 12229−12239.

(22) Nilges, M.; Gronenborn, A. M.; Brunger, A. T.; Clore, G. M. Determination of the Three-dimensional Structures of Proteins by Simulated Annealing with Interproton Distance Restraints. Application to Crambin, Potato Carboxypeptidase Inhibitor and Barley Serine Proteinase Inhibitor 2. *Protein Eng.* **1988**, *2*, 27−38.

(23) Brunger, A. T. *XPLOR Manual*, version, 3.1; Yale University Press: New Haven, CT, 1993.

(24) Moseley, H. N. B.; Monleon, D.; Montelione, G. T. Automatic Determination of Protein Backbone Resonance Assignments from Triple Resonance Nuclear Magnetic Resonance Data. *Methods Enzymol.* **2001**, *339*, 91−108.

(25) Constantine, K. L.; Mueller, L.; Goldfarb, V.; Wittekind, M.; Metzler, W.; Yanchunas, J.; Robertson, J. G.; Malley, M. F.; Friedrichs, M. S.; Farmer, B. T. Characterization of NADP+ Binding to Perdeuterated MurB: Backbone Atom NMR Assignments and Chemical-shift Changes. *J. Mol. Biol.* **1997**, *267*, 1223−1246.

(26) Grzesiek, S.; Vuister, G. W.; Bax, A. A Simple and Sensitive Experiment for Measurement of JCC Couplings between Backbone Carbonyl and Methyl Carbons in Isotopically Enriched Proteins. *J. Biomol. NMR* **1993**, *3*, 487−493.

(27) Breeze, A. L. Isotope-Filtered NMR Methods for the Study of Biomolecular Structure and Interactions. *Prog. Nucl. Magn. Reson. Spectrosc.* **2000**, *36*, 323−372.

(28) Friedrichs, M. W.; unpublished program.

(29) Marion, D.; Ikura, M.; Bax, A. Improved Solvent Suppression in One-and Two-Dimensional NMR Spectra by Convolution of Time-Domain Data. *J. Magn. Reson.* **1989**, *84*, 425−430.

(30) Wishart, D. A.; Bigam, C. G.; Yao, J.; Abildgaard, F.; Dyson, H. J.; Oldfield, E.; Markley, J. L.; Sykes, B. D. ^{1}H, ^{13}C and ^{15}N Chemical Shift Referencing in Biomolecular NMR. *J. Biomol. NMR* **1995**, *6*, 135−140.

(31) Friedrichs, M. W.; Mueller, L.; Wittekind, M. An Automated Procedure for the Assignment of Protein ^{1}HN, ^{15}N, $^{13}C^{\alpha}$, $^{1}H^{\alpha}$, $^{13}C^{\beta}$ and $^{1}H^{\beta}$ Resonances. *J. Biomol. NMR* **1994**, *4*, 703−726.

(32) *MacroModel V91106*; Schrodinger, LLC, New York. http://www.schrodinger.com/.

(33) Still, W. C.; Tempczyk, A.; Hawley, R. C. Semianalytical Treatment of Solvation for Molecular Mechanics and Dynamics. *J. Am. Chem. Soc.* **1990**, *112*, 6127−6129.

JM060360I